Low-Power MIMO Guided-Wave Communication

CHRISTIAN KEXEL[ID][1], **NICOLA TESTONI**[ID][2], **FEDERICA ZONZINI**[ID][2], **(Student Member, IEEE)**,
JOCHEN MOLL[ID][1], **AND LUCA DE MARCHI**[ID][3], **(Member, IEEE)**
[1]Department of Physics, Goethe University Frankfurt, 60438 Frankfurt, Germany
[2]Advanced Research Center on Electronic Systems, University of Bologna, 40136 Bologna, Italy
[3]Department of Electrical, Electronic, and Information Engineering, University of Bologna, 40136 Bologna, Italy

Corresponding author: Christian Kexel (christian.kexel@physik.uni-frankfurt.de)

ABSTRACT This article demonstrates the use of guided elastic waves (GEW) for multiple-in and multiple-out (MIMO) data communication in the framework of a structural health monitoring (SHM) system. Therefore, miniaturized low-voltage communication nodes have been developed. They are arranged in a spatially distributed and permanently installed network. Wireless exchange of encoded information across a metallic plate and a stiffened carbon-fiber reinforced plastics (CFRP) structure is investigated. A combination of square-wave excitation sequences and frequency-division multiplexing (FDM) is explored for parallel communication with multiple nodes. Moreover, the impact of the excitation-sequence length on the reliability of information transmission is studied in view of future energy-aware application scenarios. The presented system achieves in both studied structures error-free transmission at a data rate of 0.17 kbps (per carrier frequency) with a power consumption of 224 mW.

INDEX TERMS Lamb waves, structural health monitoring, digital communications.

I. INTRODUCTION

Detecting, localizing and classifying structural defects in an automated manner are the key purposes of conventional SHM systems. Here, GEW represent an appealing tool for monitoring non-destructively the condition of thin mechanical components. For an introduction and background regarding SHM and GEW the reader is referred to the available recent literature [4], [9], [19], [23], [37]. Lamb waves are one type of GEW, which are sensitively scattered by specific types of damage, including cracks [18], [26], disbonding [21], delaminations [32] or impact damage [17]. Furthermore, they undergo merely moderate energy dissipation and therefore reach comparatively large distances. Guided-wave SHM systems commonly comprise a distributed array of transducers, which is permanently installed on or in the technical structure [11], [19]. Prescinding from the non-destructive monitoring functionality, the inherent complementary capability of the transducers to transmit information between the array's transducer nodes might be deployed in next-generation SHM systems. Here, the technical structure itself functions as the physical layer for wave propagation and communication. This new complementary feature might be practical when conventional wireless electromagnetic or cabled communication is

not viable or too expensive, i.e. in lightweight, underground or underwater applications. When those standard communication techniques are prohibitive and high-speed transmission is dispensable, GEW-based data transmission can be a compelling alternative. The wireless communication capability might become an essential part of future intelligent systems [7], where the distributed nodes of the SHM systems share information, e.g. a damage-indicating metric, so as to eventually deliver this information to a base station for further analysis. In SHM systems, the damage indicator is a numerical value which enables detecting the emergence of a damage over time. Examples are discussed e.g. in Ref. [2]. However, apart from reaching large distances and the sensitivity towards specific types of defects, it is worth stressing that Lamb waves show intricate behavior while propagating. In fact, they might

1) show different wave modes,
2) exhibit dispersive behavior, i.e. a change in wave speed depending on the excited mode, excitation frequency, thickness of the waveguide and the material characteristics of the structure,
3) be affected by mode conversion,
4) yield reverberations leading to multipath signals.

In spite of the above impediments, reliable acoustic communication is feasible across a variety of different structural components. The theoretical data rates have been in the

---

The associate editor coordinating the review of this manuscript and approving it for publication was Jenny Mahoney.

order of tens or hundreds of kbps, which should be high enough for most of the envisioned future applications. Node-to-node communication across a metallic plate has been simulated numerically in [24] where single-mode Lamb waves have been employed for parallel transmission of encoded information from multiple piezoceramic transducers (PZTs) by combining phase modulation with code division multiplexing. Dispersion compensation has been applied to the measured signals before decoding the transmitted information. Additional calculations have been performed to investigate the aforementioned communication scheme in a tapered waveguide [8]. Proof-of-principle experiments with/without dispersion compensation have been carried out for an aluminum plate in [25]. Moreover, the impact of structural damage on the communication quality employing amplitude modulation (AM) and multi-modal Lamb waves has been studied numerically as well as experimentally in [16]. In [15], successful transmission of digital data by way of this AM scheme has also been demonstrated in practical scenarios, specifically concerning two spatially separated planar wave-guides, which were in contact solely through a movable metal piece. This correlation-based AM approach has been tested in rather complex technical components, such as a composite helicopter rotor blade and a sandwich panel [27]. In [14], wireless delivery of encoded information through a glass-fiber reinforced polymer planar waveguide has been studied by the time-domain AM-based scheme and frequency-division multiplexing (FDM) schemes. A recent study also includes a medical application: in [28], the transmission of fracture-related information is discussed, where data from a PZT fixed to the surface of a bone is sent to an acoustic receiver located externally on the skin surface.

Relevant recent research comprises the combination of pulse-position modulation (PPM), where the time delay between pulses bears information, and the time-reversal processing [12], which is able to compensate for dispersion and multiple wave modes. However, MIMO communication involving multiple interfering nodes cannot be accomplished using this concept. In addition, PPM has been deployed for ultrasonic information transmission through one-dimensional waveguides [34], [35], namely multiwire cables. A low-rate communication approach using chirped AM has also been investigated for communicating digital data across a cylindrical structure [5]. Acoustic communication across tubular parts of an undersea oil platform [22] and water pipelines [13] have been moreover presented. In [31], AM and orthogonal FDM have been tested amongst others utilizing a variety of solid channels, including blocks, plates, and pipes.

In the present research work, the wireless delivery of encoded information through a metallic planar waveguide as well as a stiffened CFRP structure is investigated. In detail, novel low-voltage communication nodes employing a combination of square-wave excitation with FDM were employed, enabling for parallel emission from multiple distributed nodes. As a proof-of-principle, two transmitters and two receivers are considered. The possibility to send and receive

in parallel is the basic functionality of MIMO. First, MIMO is beneficial to increase the reliability/robustness of the communication by allowing spatially separate links. Secondly, MIMO enables increasing the amount of information that can be shared in each time interval by using simultaneous transmission. These are the two main motivation for evaluating MIMO. The evaluation concentrates on a metal structural component, because metallic parts are of eminent relevance in the field of non-destructive evaluation and thus also of SHM [29]. Further experiments are presented from a composite panel as a complex and also practically relevant structure. Parts of these studies already appeared as a conference contribution [3]. The novelty of the research work presented here consists of:

1) Experimental demonstration of the ability to communicate in parallel between adjacent nodes using GEW
2) Testing of miniaturized and distributed communication nodes
3) Exploitation of a low-level communication protocol based on square-wave sequences as well as parametric investigation regarding robust data exchange
4) Physical interpretation of propagation characteristics of the fundamental modes and their higher harmonics
5) Development of dedicated signal processing for information decoding and analytics

The remainder of this article is the following: Sect. II introduces the experimental setup, whereas Sect. III covers the relevant theoretical background. Then, Sect. IV is dedicated to the experimental validation and conclusions are finally presented in Sect. V.

II. EXPERIMENTAL SETUP
MIMO communication is primarily studied across an aluminum plate, then the approach is replicated on a more challenging CFRP component.

A. METALLIC STRUCTURE
A small communication network comprising two transmitter nodes (Tx1 and Tx2) and two receiver nodes (Rx1 and Rx2) was realized on a 1000 mm × 1000 mm wide, 3 mm thick, aluminum plate. As shown in Fig. 1, the nodes are positioned at the vertex of a square, 140 mm apart from each other, 220 mm from the border, in the bottom right quadrant of the plate.

Each communication node comprises a multi-channel PZT with three active regions and an electronic board hosting all the circuitry necessary for the low-voltage excitation and acquisition of the electric signal generated by the PZT. The hardware of the communication nodes, shown in Fig. 2, was designed to be characterized by low weight (less than 5 g), small size (30 mm × 23 mm) and low current consumption (44.8 mA) at a voltage of 5 V. Thanks to these features, the acquisition system is suitable for smart and long-term structural monitoring.

Taking steps from a previous realization [33], each communication node is based on a ST-Microelectronics
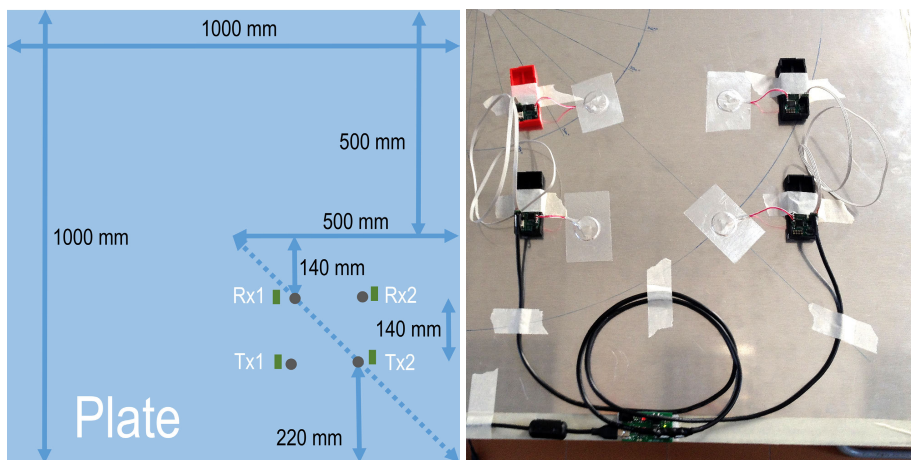
FIGURE 1. Dimensions (left) and arrangement (right) of the metal-plate setup including the two transmitters (Tx1, Tx2) and the two receivers (Rx1, Rx2) adjacent to the circular PZTs, and the gateway (bottom middle on the right picture).
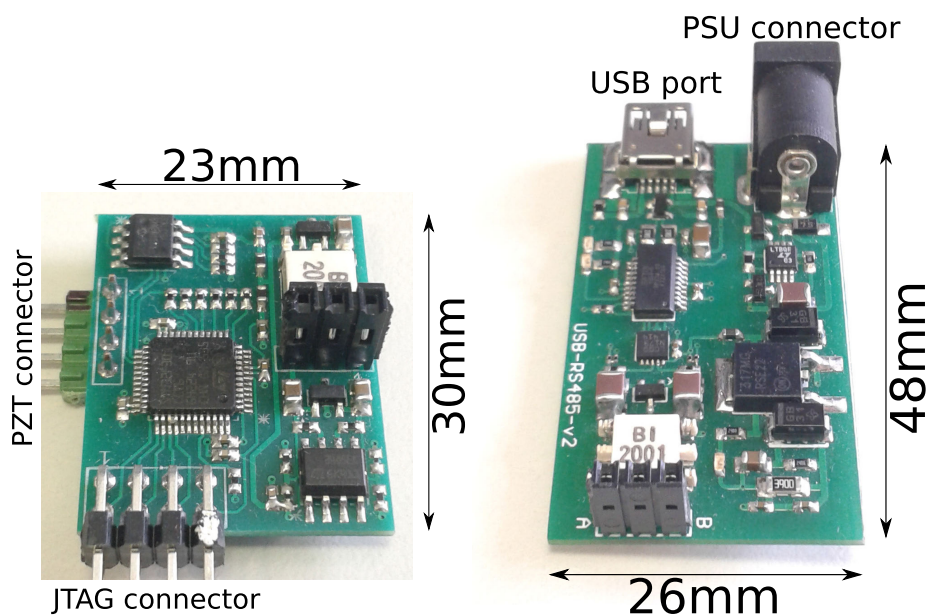

FIGURE 2. Close-up photograph of the communication node (left) and interface (right) used in this work to actuate and detect GEW.

Microcontroller Unit (MCU) STM32F3 which embeds four rail-to-rail, 8.2 MHz operational amplifiers with external or internal follower routing, programmable gain, and filter capabilities. Four rail-to-rail 0.2 µs analog-to-digital-converters with selectable integrated voltage reference are available: they allow for the simultaneous conversion of up to four analog input signals characterized by a 12 bit precision obtained via successive approximations. Moreover, two 12 bit digital-to-analog channels are also available: one of them is used to provide low voltage polarization to the PZT, the other for PZT auto-diagnostic purposes. High speed general-purpose I/O drivers are used to drive the PZT for data transmission purposes. The nodes were placed as close as possible to the PZTs to reduce electromagnetic noise to the minimum.

All the communication nodes are connected in a daisy-chain fashion by means of a Sensor Area Network

(SAN) bus exploiting data-over-power (DoP) communication, with a synchronicity error less than 50 µs. Meaningful information is exchanged with a PC connected through a gateway interface, also illustrated in Fig. 2. Within this device, a FTDI FT231X USB to full-handshake universal asynchronous receiver-transmitter (UART) integrated circuit is used to provide USB (universal serial bus) connectivity to the PC, whereas a ST-Microelectronic ST3485EB RS485/RS422 transceiver is used to interface the UART to the SAN network. Each interface node is roughly 48 mm × 26 mm wide, weights less than 10 g, and consumes 12 mA, making it attractive for application scenarios where size, power, and weight reduction are crucial.

These devices have been used to actuate and detect low-energy GEW. During the experiment, transmitter nodes were programmed to emit a finite-length sequence of

rectangular pulses with a 50% duty cycle. Utilization of rectangular pulses is motivated by the fact that they are readily implemented using energy-aware digital hardware. Besides transmission, receiver nodes were programmed to acquire at the same time 6 ms of data at a sample rate S of 500 kSps. Two channels for each transmitter node were used to excite different carrier frequencies by means of digital pulses. Linear superposition of effects was used to simultaneously inject up to four different signals into the structure.

By exploiting the amplification stage embedded into the receiver nodes, and carefully choosing the transmitted carrier frequencies, a peak-to-peak voltage of 387 mV was measured in the received signal in correspondence of an actuation peak-to-peak voltage of 3.3 V. The amplitude of the excited pulses in the experiments thus corresponds to the aforementioned voltage value. In absence of any transmitted signal, the maximum peak-to-peak voltage of the received signals was 6.03 mV. Each test was repeated 10 times to assess the robustness against noise and jitter: the median absolute deviation of the recorded signals with respect to the median signal is 5.44 mV.

B. CFRP STRUCTURE

In Fig. 3, the above-described hardware is mounted onto a CFRP plate so as to investigate data transmission across a structure which exhibits anisotropy, stronger attenuation and potentially mode conversion. The stiffener which is attached to the CFRP plate is shown in an inset in the top-left corner of Fig. 3. The composite panel has the same dimensions as the aluminum plate: it is 1000 mm × 1000 mm wide and 3 mm thick.
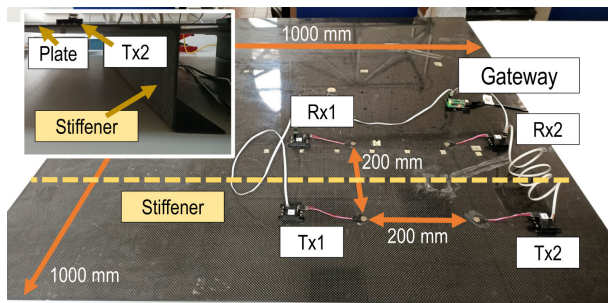

FIGURE 3. Experimental setup regarding the CFRP plate having a stiffener (sideview as inset).

III. THEORETICAL BACKGROUND

The following section covers the basics of the parallel communication approach together with the spectral properties of the square-wave excitation and the characteristics of GEW propagation.

A. FREQUENCY-DIVISION MULTIPLEXING

GEW are exploited for transmission of digital data across structures. FDM uses the bandwidth of the mechanical waveguide for communicating in parallel at multiple carrier frequencies. Here, the FDM approach from [14]

is utilized. The aforementioned strategy is illustrated in Fig. 4, where simple sinusoidal signals are shown for the sake of clarity. The next section discusses the actually employed square-wave excitation mechanism, according to which a set of carrier frequencies is assigned to each involved node and where a single frequency represents one bit. Correspondingly, the set which belongs to a distinct node is standing for a complete digital message that this particular node is able to send at a time.
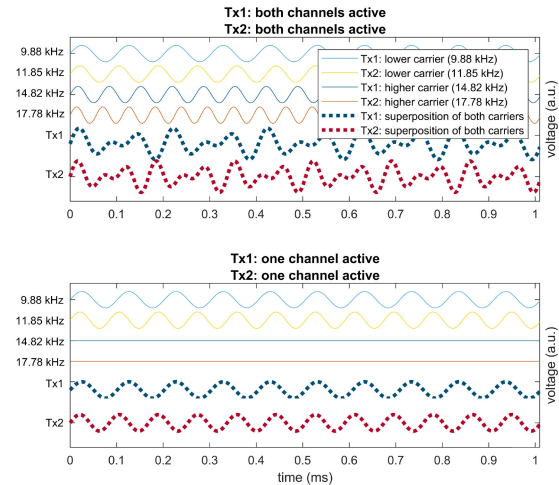

FIGURE 4. Examples of FDM using two transmitters (Tx1, Tx2) having two channels each (one lower and one higher frequency). The output (bold dotted) of a transmitter is hence a superposition of both its carrier signals (solid lines). For simplicity, sinusoidal excitations are depicted here.

B. MODULATION

Hence the frequency domain is exploited for multiplexing and modulation is accomplished through on-off keying in the time domain. Time is thus divided into equidistant intervals where transmitting with a certain carrier frequency encodes the binary value '1' and omitting transmission at this particular frequency represents the binary value '0'. A message is thus created through the linear superposition of several single-carrier excitations. The aforementioned superposition can either be realized mathematically when a single actuator emits the already-completed superposition, as in [14], or it can be realized physically by a multi-channel actuator that is fed independently by multiple singe-carrier signals. The latter variant is considered in the present work.

At the listening nodes, the spectrum of an acquired signal is probed for the absence or presence of a particular carrier frequency. If the intensity in the surrounding of the carrier is higher than the noise level, then the value '1' is considered, otherwise the binary value '0' is assumed. In this work, the full spectrum of the acquired signal is computed via a Fourier Transform. Nonetheless, in future applications more efficient approaches, such as the Goertzel algorithm [30], might be implemented for probing the spectrum solely at a few frequencies. In general, it is possible to implement orthogonal FDM (OFDM) so as to exploit the available
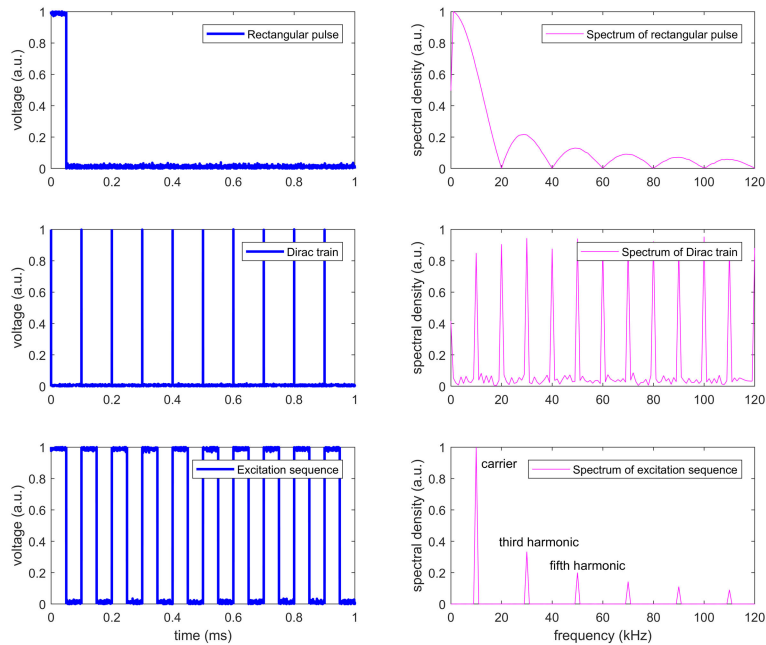
FIGURE 5. Expected spectrum of an illustrative square-wave excitation sequence (bottom) which can be regarded as convolution of a rectangular pulse (top) with a Dirac train (middle).

bandwidth more efficiently, but it is beyond the scope of our proof-of-principle. Requiring orthogonality in OFDM would introduce more complexity, e.g., regarding the signal processing as OFDM is usually deployed using cyclic prefixes and on-node Fourier transforms.

C. JOINT OPTIMIZATION OF EXCITATION-SEQUENCE LENGTHS

In the present work, for each of the 4 communication links, only one carrier frequency is considered. However, according to the FDM approach outlined above, in general, a whole set of carriers might be deployed. In order to select specific frequencies $f_1^{(1)}$ to $f_4^{(1)}$, an optimization procedure has been performed. In our scenario, the number of communication links is $N = 4$. For a given communication link i the excitation-sequence length L_i is defined by the number of times one rectangular pulse is repeated. Hence, L_i is equivalent to the number of excitation cycles of a conventional tone-burst if sinusoidal actuation would have been considered here. The duration of a single rectangular pulse is denoted t_i and commonly dubbed pulse width. Considering a 50% duty cycle, the excitation-sequence duration is $T_i = 2 \cdot t_i \cdot L_i$. For communication scenarios where a global clock, gating or synchronization between the N communication links is desirable, any two excitation sequences i and j may jointly be optimized to possess equal duration $T_i = T_j$. In that case, the index can be dropped: T. Such a joint optimization of excitation-sequence lengths L_i has been performed, which aimed at two objectives: (i) a duration T_i as short as possible and hence a maximal length $\max_i (L_i) = L_4$ as short as possible. Furthermore, (ii) equidistance between carrier

frequencies $f_i^{(1)}$ is desired. For the carrier frequency $f_i^{(1)} = \frac{F}{2 \cdot t_i} = \frac{S}{T} \cdot L_i$ holds, where S denotes the sample rate. Hence, $f_i^{(1)} \propto L_i$ holds. Thus the desired equidistance between carriers can be expressed as a deviation of the differences $\Delta_{ij} = L_i - L_j$ as small as possible. Therefore a normalized root-mean-square deviation (nRMSD) can be defined as

$$\frac{1}{\bar{\Delta}} \sqrt{\frac{1}{3} \left((\Delta_{43} - \bar{\Delta})^2 + (\Delta_{32} - \bar{\Delta})^2 + (\Delta_{21} - \bar{\Delta})^2 \right)} \quad (1)$$

with $\bar{\Delta} = \frac{1}{3}(\Delta_{43} + \Delta_{32} + \Delta_{21})$.

Finally, the optimization problem can be stated in the following way where $T_i = \text{const.}$:

$$\min_{L_i} (\text{nRMSD}(L_i), L_4) \quad \text{s.t.} \quad L_4 < 2 \cdot L_1 \quad (2)$$

Since a multitude of candidate solutions exist for this combinatorial problem, an additional constraint has been introduced: the highest carrier frequencies within the set is required to lie below the second harmonic of the lowest carrier.

D. SQUARE-WAVE EXCITATION

The nodes are supposed to excite a square-wave sequence that is used in the aforementioned FDM approach for GEW-based communication across a mechanical waveguide. Subsequently, at the receiver, the spectrum is analyzed. In Fig. 5 the spectrum that can be expected from a square-wave sequence is plotted. Note that the situation prior to the propagation through the solid is depicted and thus dismissing phenomena, such as frequency-dependent attenuation. In general, any square-wave excitation sequence can
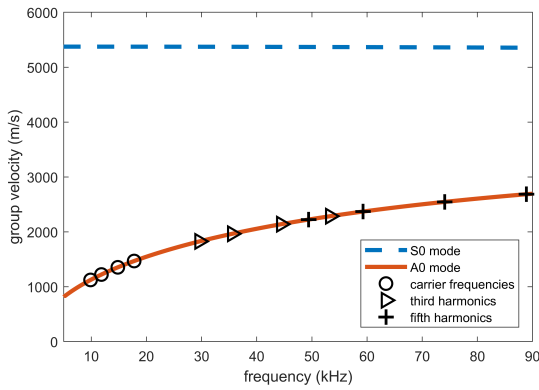
FIGURE 6. Simulated Lamb-wave dispersion plot showing the symmetric and the dominant antisymmetric mode in the aluminum plate where the harmonics of the frequencies used in the experiment (triangles, crosses) are expected to have higher speed than the carriers (circles).

be regarded as the mathematical convolution of a rectangular pulse with a so-called Dirac train. This fact formally reads as $\mathbf{s}(t) = \mathbf{s}_{\text{Rect}}(t) * \mathbf{s}_{\text{Dirac}}(t)$. Hence, due to the renowned Convolution Theorem, its Fourier transform is given by the product of the constituting signals' Fourier transforms:

$$F\{\mathbf{s}(t)\} = F\{\mathbf{s}_{\text{Rect}}(t) * \mathbf{s}_{\text{Dirac}}(t)\}$$
$$= F\{\mathbf{s}_{\text{Rect}}(t)\} \cdot F\{\mathbf{s}_{\text{Dirac}}(t)\} \qquad (3)$$

Here, $F\{\mathbf{s}(t)\}$ denotes the Fourier transform of time-domain signal $\mathbf{s}(t)$. From Fig. 5 it can be seen that besides the carrier frequency, denoted by $f^{(1)}$, also odd-numbered harmonics $f^{(3)}, f^{(5)}, \dots$ are present in the spectrum. The intensity due to the harmonics can be exploited for the presented FDM approach where not only the vicinity of the carrier is probed, but also the spectral portions around the harmonics are checked.

E. LAMB-WAVE PROPAGATION
The PZTs that are attached to the structure are able to excite GEW which subsequently propagate through the mechanical waveguide and eventually reach the receiver where the waves are sensed. Lamb-type waves are the kind of GEW that are relevant for the present work. In general, Lamb waves might exhibit two types of modes that are dubbed symmetric and antisymmetric. Starting from low frequencies, the fundamental modes are the first and only modes which can exist. They are denoted S0 and A0, respectively. It is well-known that at low frequencies the A0 mode is dominant and that the S0 mode will emerge with increasing frequency [10]. Lamb waves are dispersive as demonstrated in Fig. 6 where the theoretical group velocity is plotted for both fundamental modes. Here, the material properties and the geometry of the presented aluminum plate are considered. The dispersion diagram has been calculated using the GUIGUW program [20]. The dispersive nature of Lamb waves is well understood and efficient numerical methods are available for plotting dispersion diagrams regarding a variety of geometries of (an)isotropic and layered structures [1], [20].

While the dispersion is well-studied, no similar understanding/theory exists for the absorption behaviour of Lamb waves. In Fig. 6, in the depicted regime the A0 mode is highly frequency-dispersive which leads to an interesting phenomenon: if harmonics are excited through the described square waves, then the harmonics will travel with increased speed. Nevertheless, the intensity of the harmonics is less pronounced than the intensity of the carrier frequency (see Fig. 5).

From the considered spatial, time and velocity scales (see Figs. 1, 3 and 6), it is evident that this work deals with travelling waves instead of standing waves. A standing wave will not built up, because primary waves and reflections do not overlap substantially. For example, the typical excitation sequences span a duration of roughly 1 ms and the travel distance for reflections is in the order of 1 m, therefore from the wave speeds of the carriers (closely above 1000 m/s), it can be deduced that excitation terminates around the time when reflections arrive.

IV. RESULTS AND DISCUSSION
A. SIGNAL ANALYSIS
The communication approach studied in this work relies on the spectral properties of Lamb waves. Considering Lamb waves in the frequency-domain alleviates the challenges which are due to their inherent intricate propagation behavior and the additional complexity related to the generation of harmonics. This non-trivial waveform is demonstrated in the following: as a first step, a square-wave excitation sequence of length 1 is studied, which corresponds to a single rectangular pulse (and is analogous to an one-cycle tone-burst if conventional sinusoidal excitations had been used). On the left-hand side of Fig. 7, a distinct signal related to the aluminum plate is analyzed in the time domain and the individual causal contributions are highlighted.

In order to further inspect the overlapping contributions and in order to support a detailed understanding of the isotropic metal-plate setup, a finite-element simulation [36] has been carried out. The simulation has been accomplished using the COMSOL software package [6]. A snapshot of the wavefield is presented in Fig. 8. In contrast to the causal decomposition that is shown on the left-hand side of Fig. 7, the right-hand panel of Fig. 7 demonstrates that a visual-based inspection of the signals does not provide insight on such a separation of causal contributions when typically measured signals are dealt with.

B. JOINT OPTIMIZATION OF EXCITATION-SEQUENCE LENGTHS
Results of the optimization procedure are depicted in Fig. 9.

Candidate solutions lying on the Pareto front are additionally detailed in Tab. 1. When the sequence length is set, then the carrier frequency can be adjusted by specifying the pulse width t_i.
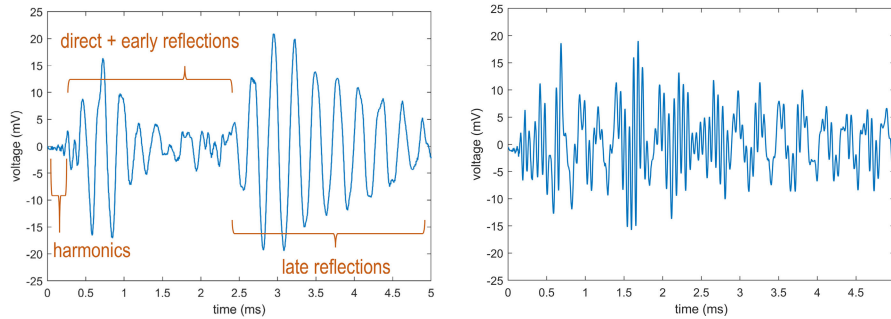
FIGURE 7. Illustrative time-domain signals from the experimental measurements involving the aluminum plate. Left: Single-pulse signal sent from Tx1 with $f_1^{(1)} = 9.88$ kHz and recorded at Rx2. Early-arriving power stems from harmonics which are faster than the antisymmetric mode having the carrier frequency. The direct, primary wave overlaps with back and lateral reflections from adjacent edges of the plate. The late signal content originates from reflections at the distant edges of the plate. Right: Single-pulse signal sent from Tx2 with $f_4^{(1)} = 17.78$ kHz and recorded at Rx1.
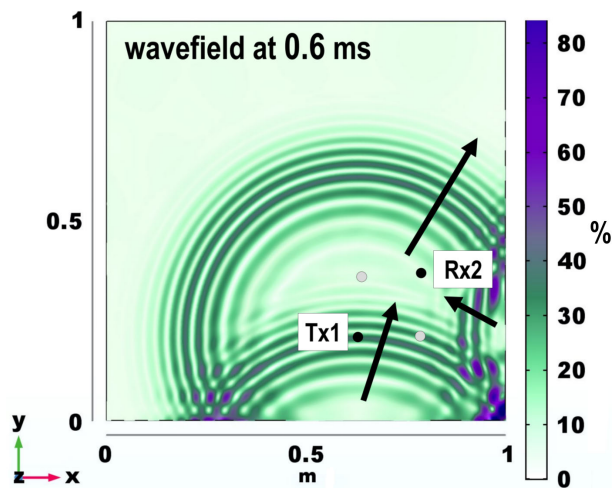

FIGURE 8. Simulated wavefield of a rectangular-pulse signal sent from Tx1 with $f_1^{(1)} = 9.88$kHz showing the incidence of the early reflections right after the direct wave has passed Rx2 on the aluminum plate. Surface stresses are expressed in terms of percentage relative to the initial amplitude.

TABLE 1. A listing of the Pareto-optimal lengths. A duty cycle of 50% is assumed throughout. Subsequently fixing the duration of a single pulse will hence define the actual carrier frequency of the excitation.

L_1	L_2	L_3	L_4	nRMSD
8	10	12	15	0.20
10	12	15	18	0.18
14	18	21	24	0.14
21	24	28	32	0.13

C. STUDY OF EIGENMODES OF THE METAL PLATE

It is noteworthy that carrier choice can be guided by the possibility to exploit eigenmodes of the system in order to reduce power consumption of the electronics. The finite-element model of the described aluminum plate is thus used so as to compute eigenmodes λ_k of the mechanical waveguide. COMSOL is utilized again. Results are provided in Tab. 2. In contrast, for the CFRP structure the numerical evaluation is more delicate and thus an empirical carrier selection is discussed in Sect. IV-D2.
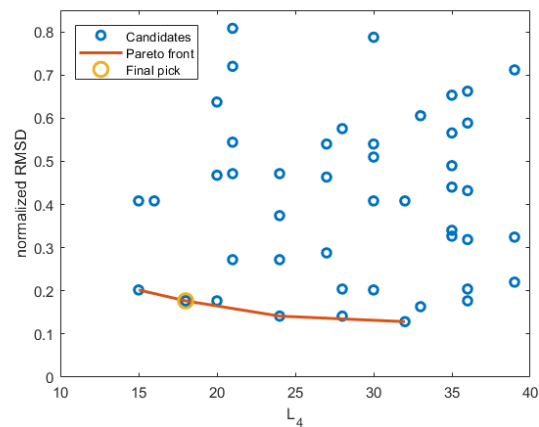

FIGURE 9. Optimization of same-duration excitation sequences. The final pick of the excitation-sequence lengths $L_i \in \{10, 12, 15, 18\}$ is Pareto optimal regarding minimal length L_4 and equal spread given by the normalized root-mean-square deviation.
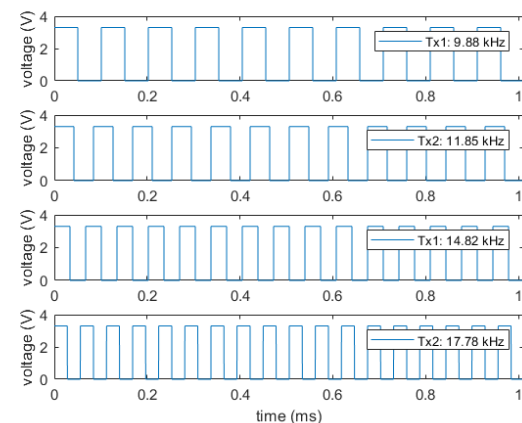

FIGURE 10. Depiction of the same-duration excitation sequences used in the aluminum-related experiment.

D. BIT RECONSTRUCTION PERFORMANCE

This section is divided into a part devoted to the metallic waveguide followed by a second discussion concerned with the analysis of the composite panel.
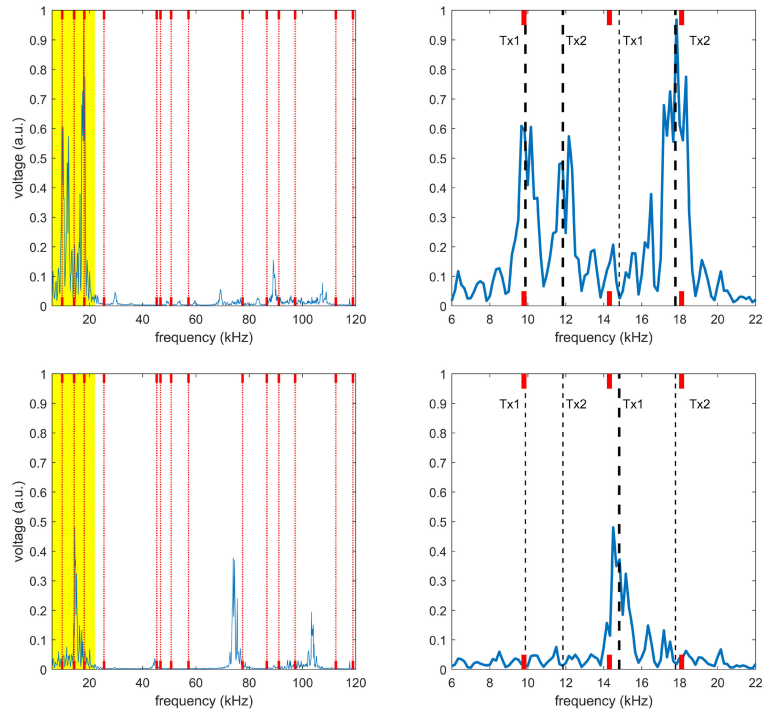
FIGURE 11. Exemplary spectra with different active channels for the aluminum plate. Left: Spectrum including harmonics where red lines indicate location of the plate's eigenmodes. Right: Magnification with bold vertical lines indicating active channels and red bold ticks indicating the first three eigenmodes.

TABLE 2. Eigenmodes (in kHz) of the aluminum plate.

λ_1	λ_2	λ_3	λ_4	λ_5	λ_6	λ_7
9.8	14.3	18.1	25.5	45.3	46.7	50.7

λ_8	λ_9	λ_{10}	λ_{11}	λ_{12}	λ_{13}	λ_{14}
57.2	77.5	86.6	91.1	97.2	112.5	118.9

1) METALLIC STRUCTURE

The selected same-length square-wave excitation sequences that are going to be used for the following experimental investigation are shown in Fig. 10 and are taken from the second row of Tab. 1. The excitation sequences correspond to bursts having 10, 12, 15 and 18 cycles.

Exemplary spectra of the recorded GEW signals are depicted in Fig. 11 where intensity arriving at Rx1 and Rx2, respectively, is summed. In the lower row of Fig. 11, the fifth harmonic of the carrier is very pronounced as compared to its third harmonic or as compared to all the harmonics in the upper row of the same figure. This observation highlights the effect which the propagation through the solid waveguide can have on the spectrum.

A quantitative analysis is carried out which accounts for the $2^4 = 16$ possible combinations of active channels. The intensity that is present in the spectrum when the channel is off is compared to the intensity of an active channel. Results are given in Tab. 3. This analysis illustrates that a clear discrimination can be achieved between active and inactive communication links. Formally, this fact is indicated by an inactive-active ratio below 1.

2) CFRP STRUCTURE

Similar analysis is carried out for the CFRP structure. Since the inherent complexity of the structure makes the numerical study of the eigenmodes a challenging and time-consuming task, firstly the indication of eigenmodes has been omitted in Fig. 12 and secondly an empirical approach was followed to estimate the optimal set of carrier frequencies. More specifically, exploiting the advantageous capability of the developed circuitry to generate custom signals, pseudo-random digital sequences were repeatedly transmitted by means of an active transducer operating at a symbol rate $F_{sym} = 200$ kHz (i.e. $T_{sym} = 5\mu s$) and recorded by a passive transducer operating at a sampling frequency $F_{smp} = 2$ MHz. Such an operating value was chosen to be sufficiently flat in the frequency band of 0 - 100 kHz, ensuring an oversampling factor of ten compliant with a Nyquist spectral window of 1 MHz. Accordingly, the frequencies to be selected correspond to the most energetic peaks in the spectrum of the received signals while also considering equal spread (as discussed in Sect. IV-B). Such an empirical frequency selection procedures has already been recently proposed [14]. In Fig. 13, which represents the average spectrum obtained from 99 pseudo-random noise repetitions, the selected carriers (10.70 kHz, 12.84 kHz, 16.00 kHz, 19.25 kHz) are depicted. Here, the excitation sequences correspond to bursts having 10, 12, 15 and 18 cycles (see second row of Tab. 1). As such, this set of frequencies was then set during the experimental campaign on the CFRP structure.
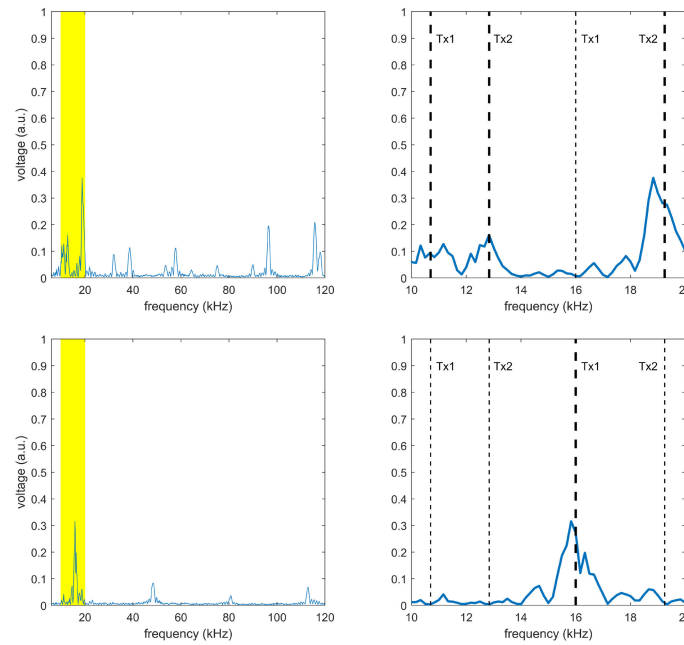
FIGURE 12. Exemplary spectra with different active channels for the CFRP panel. Left: Spectrum including harmonics. Right: Magnification with bold vertical lines indicating active channels where the same scale is used as in Fig. 11.
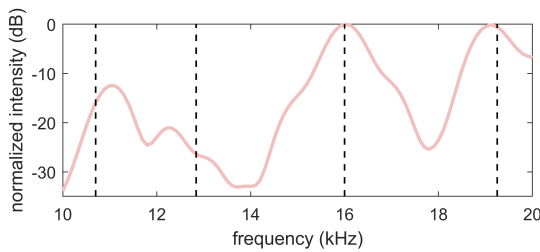

FIGURE 13. Spectrum of the CFRP structure received from noisy actuation. The four selected carriers (dotted lines) again represent a trade-off between exploitation of the most energetic peaks and a sufficient spread of the carriers.

FIGURE 14. Ratio of measured intensity in the spectrum as function of power that is fed into excitation for the aluminum plate. The intensity is accumulated in a bin (width 2 kHz) around the carrier frequency and also its harmonics (up to the ninth). Intensities are compared for cases where the distinct channel is inactive and cases when it is actively transmitting. A ratio below 1 allows perfect discrimination between inactive and active. Plots include an average scenario (solid) and a worst-case assessment (dotted line). For the latter, among all measurements the maximal inactive intensity is compared to the minimal active intensity.

In Fig. 12 the intensity received at the sensors is reduced as compared to the aluminum plate due to the stronger attenuation in the waveguide. Moreover, on the left-hand side of Fig. 12, it can be observed that the higher harmonics are all very pronounced in the CFRP plate as opposed to the very selective excitation in the metallic structure.

Even though the received intensity is lessened in the CFRP panel (as justified by a comparison of the spectral magnitudes of Fig. 12 opposed to those of Fig. 11), the bit reconstruction (in terms of a lower inactive-active ratio) can nevertheless be sharper than in the aluminum plate for certain carrier frequencies (i.e. $f_3^{(1)}$ in Tab. 3). Since the inactive-active ratio is again below 1, in this measurement an error-free recovery is achieved for every carrier.

E. IMPACT OF SEQUENCE LENGTH ON BIT RECONSTRUCTION

The influence of sequence length on the quality of the communication links is further investigated, firstly tackling the
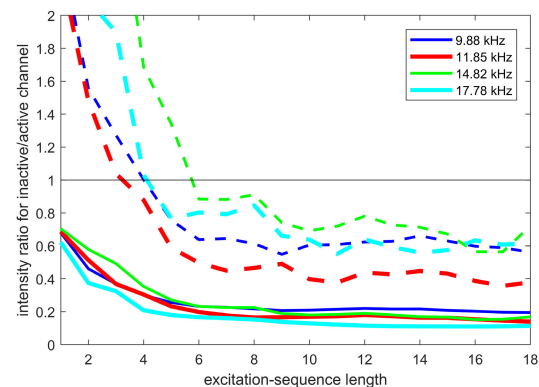
transmission potentialities of the metallic plate and then moving to the more complicated CFRP structure.

1) METALLIC STRUCTURE

Bit reconstruction, namely the discrimination between a communication link that is on versus a link that is off, is feasible for the above same-length sequence. Additionally, a similar analysis is performed for varying length of the square-wave excitation signal. Again, all 16 combinations have been probed and moreover, measurements were repeated 10 times. Results are depicted in Fig. 14 where perfect reconstruction

TABLE 3. Comparison of normalized spectral intensity that is accumulated in a bin (width 2 kHz) around the carrier frequencies at both receivers.

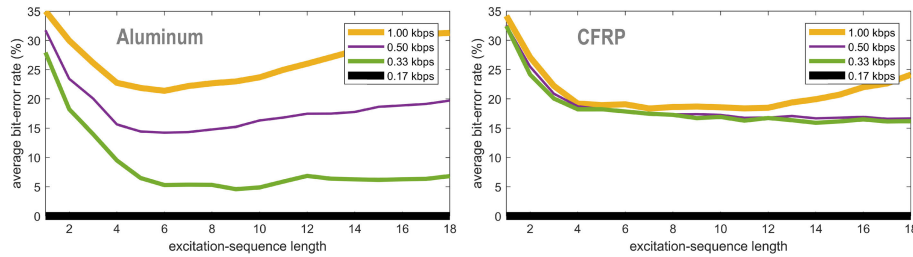|	Aluminum				CFRP			
	$f_1^{(1)}$	$f_2^{(1)}$	$f_3^{(1)}$	$f_4^{(1)}$	$f_1^{(1)}$	$f_2^{(1)}$	$f_3^{(1)}$	$f_4^{(1)}$
channel inactive	0.09	0.08	0.12	0.07	0.06	0.02	0.04	0.03
channel active	0.63	0.55	0.43	1.00	0.12	0.14	0.29	0.40
inactive-active ratio	0.14	0.15	0.29	0.07	0.45	0.17	0.14	0.08

FIGURE 15. Average bit-error rate as function of excitation length and data rate per frequency for the aluminum plate (left) and the CFRP structure (right). In both structures error-free communication is hence possible at a data rate of 0.17 kbps per carrier.

is successful for lengths equal to and above 6 rectangular pulses. On average the reconstruction works already for a single pulse. Here it is assumed that the full recorded signal of 6 ms duration is processed. Illustrative signals are plotted in Fig. 7. This duration hence corresponds to a data rate of 0.17 kbps per frequency, if one follows the approach to encode a bit in the time domain through temporal activation or deactivation of a certain carrier. The bit duration, also referred to as symbol duration, of 6 ms consists in the actuation and a guard interval. For example, if a carrier frequency of 9.88 kHz is chosen and excitation length 6, then actuation of one bit solely spans 0.607 ms. Increasing the data rate by reducing the processed signal duration, accordingly deteriorates bit reconstruction, because each bit is contaminated with signal intensity stemming from the late signal content of the previous bit. On the left-hand side of Fig. 7 the direct wave, early and late reflections are indicated which are due to the multipath propagation of the GEW. This impairing phenomenon is known as intersymbol interference.

The bit-error rate (BER) is a common figure-of-merit with respect to bit recovery. Based on the data which underlies Fig. 14, also the BER can be determined. The BER corresponds to the fraction of mis-classified bits. In this computational analysis, an optimal threshold for the measured intensity in the spectrum is set and all bits that are falsely classified are counted. That means if the distinct channel is inactive, but the intensity lies above the threshold, this case is seen as an error. In addition, if the distinct channel is active, but the intensity lies below the threshold, this is also considered a mis-classification. In the computational analysis of the BER, the processed signal duration is reduced to 1 ms, 2 ms as well as 3 ms and the spectral intensity around each carrier is contaminated artificially with the late signal content of preceding bits. For each receiving node, each of its channels and also each carrier a subset of 3200 combinations of preceding bits is sampled randomly from the available

experimental data which contains all possible active/inactive channel combinations and moreover 10 repetitions. An average is calculated from the 4 measured carriers. The results concerning this average BER are given in Fig. 15 as a function of sequence length (horizontal axis) and data rate per frequency (3 different curves; see legend). Especially for the higher data rates per frequency, it can be observed that the BER increases as the excitation length increases, because the prolonged excitation creates an additional overlapping contribution into subsequent bits. For instance, in a related study with energy-aware instrumentation [5] data rates of 0.10 kbps have been observed. This result resides in the same order of magnitude as the data rates witnessed in the above experiments. It is worth stressing that the indicated data rates represent data rates per frequency which means that the actual data rates in an application scenario dependent on the number of utilized carrier frequencies. Moreover, in order to improve the BER in future implementations, simple forward error-correction might be deployed, such as triple redundancy.

These above-mentioned results concerning the length-dependent performance are of interest regarding a potentially reduced power consumption by the nodes if the excitation duration is lowered. For the sake of an example, with a given consumption of 44.8 mA per node, sending one bit amounts to 27.2 μAs if as carrier frequency 9.88 kHz is considered with an excitation of 6 cycles, because one bit corresponds here to a duration of 0.607 ms.

2) CFRP STRUCTURE

Moreover, for the empirically determined set of carriers the length-dependent BER analysis is carried out also for the CFRP structure. Results can be found on the right-hand side of Fig. 15. Above a data rate of 0.17 kbps the BER increases abruptly for all excitation lengths. When compared to the aluminum case, the BER does not exhibit such a significant

dependence on the data rate, because those upper three curves lie rather close to one another. Despite its complexity, for the highest and second highest data rate (1.00 and 0.50 kbps) the CFRP performs similarly or sometimes better than the isotropic metal plate.

It is important to stress that the envisioned and already-mentioned application scenario for the presented communication system is a SHM setting where the nodes should transmit damage indicators, i.e. numerical values. The achieved data rates of 0.17 kpbs per frequency are considered sufficient for this task.

V. CONCLUSION

Novel miniaturized low-power electronics have been introduced for application as embedded nodes in structural health monitoring systems with dual functionality: inspection and wireless data communication. In this work, the focus lies on data communication: the parallel transmission of information across structural components using frequency-division multiplexing is discussed allowing for communication of multiple network nodes. The presented approach relies on digital excitation sequences which can readily be realized with energy-aware hardware. The reliability of information transmission is investigated showing that reliable communication is accomplished already for rather short sequences.

ACKNOWLEDGMENT

REFERENCES

[1] A. M. A. Huber and M. G. R. Sause, "Classification of solutions for guided waves in anisotropic composites with large numbers of layers," *J. Acoust. Soc. Amer.*, vol. 144, no. 6, pp. 3236–3251, Dec. 2018.

[2] J. Moll, C. Kexel, J. Kathol, C.-P. Fritzen, M. Moix-Bonet, C. Willberg, M. Rennoch, M. Koerdt, and A. Herrmann, "Guided waves for damage detection in complex composite structures: The influence of omega stringer and different reference damage size," *Appl. Sci.*, vol. 10, no. 9, p. 3068, Apr. 2020.

[3] F. Zonzini, L. D. Marchi, N. Testoni, C. Kexel, and J. Moll, "Guided-wave MIMO communication on a composite panel for SHM applications," *Proc. SPIE Health Monitor. Struct. Biol. Syst.*, vol. 11381, May 2020, Art. no. 1138136.

[4] P. Cawley, "Structural health monitoring: Closing the gap between research and industrial deployment," *Struct. Health Monitor.*, vol. 17, no. 5, pp. 1225–1244, 2018.

[5] S. Chakraborty, G. J. Saulnier, K. W. Wilt, E. Curt, H. A. Scarton, and R. B. Litman, "Low-power, low-rate ultrasonic communications system transmitting axially along a cylindrical pipe using transverse waves," *IEEE Trans. Ultrason., Ferroelectr., Freq. Control*, vol. 62, no. 10, pp. 1788–1796, Oct. 2015.

[6] *COMSOL Multiphysics Reference Manual, Version 5.3*, COMSOL AB, Stockholm, Sweden, 2017.

[7] S. Das, H. Salehi, Y. Shi, S. Chakrabartty, R. Burgueno, and S. Biswas, "Towards packet-less ultrasonic sensor networks for energy-harvesting structures," *Comput. Commun.*, vol. 101, pp. 94–105, Mar. 2017.

[8] L. De Marchi, A. Marzani, and J. Moll, "Ultrasonic guided waves communications in smart materials: The case of tapered waveguides," in *Proc. 8th Eur. Workshop Struct. Health Monit.*, 2016, pp. 1–8.

[9] C.-P. Fritzen and P. Kraemer, "Self-diagnosis of smart structures based on dynamical properties," *Mech. Syst. Signal Process.*, vol. 23, no. 6, pp. 1830–1845, Aug. 2009.

[10] V. Giurgiutiu, "Tuned Lamb wave excitation and detection with piezoelectric wafer active sensors for structural health monitoring," *J. Intell. Mater. Syst. Struct.*, vol. 16, no. 4, pp. 291–305, Apr. 2005.

[11] V. Giurgiutiu, *Structural Health Monitoring: With Piezoelectric Wafer Active Sensors*. New York, NY, USA: Academic, 2014.

[12] Y. Jin, Y. Ying, and D. Zhao, "Time reversal enabled elastic wave data communications using sensor arrays," *J. Acoust. Soc. Amer.*, vol. 134, no. 5, p. 3980, Nov. 2013.

[13] K. M. Joseph, T. Watteyne, and B. Kerkez, "Awa: Using water distribution systems to transmit data," *Trans. Emerg. Telecommun. Technol.*, vol. 29, no. 1, p. e3219, Jan. 2018.

[14] C. Kexel, T. Maetz, M. Mälzer, and J. Moll, "Digital communication across orthotropic composite components using guided waves," *Composite Struct.*, vol. 209, pp. 481–489, Feb. 2019.

[15] C. Kexel, M. Mälzer, and J. Moll, "Connecting physics to ICT: Demonstrating a data Drawbridge' by means of guided ultrasound waves," *Eur. J. Phys.*, vol. 39, no. 5, Sep. 2018, Art. no. 055806.

[16] C. Kexel, M. Malzer, and J. Moll, "Guided wave based acoustic communications in structural health monitoring systems in the presence of structural defects," in *Proc. IEEE Int. Symp. Circuits Syst. (ISCAS)*, May 2018, pp. 1–4.

[17] P. Kudela, M. Radzienski, and W. Ostachowicz, "Impact induced damage assessment by means of Lamb wave image processing," *Mech. Syst. Signal Process.*, vol. 102, pp. 23–36, Mar. 2018.

[18] P. Kudela, M. Radzienski, W. Ostachowicz, and Z. Yang, "Structural health monitoring system based on a concept of Lamb wave focusing by the piezoelectric array," *Mech. Syst. Signal Process.*, vol. 108, pp. 21–32, Aug. 2018.

[19] R. Lammering, M. Sinapius, U. Gabbert, T. Schuster, and P. Wierach, *Lamb-Wave Based Structural Health Monitoring in Polymer Composites*. Berlin, Germany: Springer, 2018.

[20] A. Marzani, E. Viola, I. Bartoli, F. Lanza di Scalea, and P. Rizzo, "A semi-analytical finite element formulation for modeling stress wave propagation in axisymmetric damped waveguides," *J. Sound Vib.*, vol. 318, no. 3, pp. 488–505, Dec. 2008.

[21] V. Memmolo, E. Monaco, N. D. Boffa, L. Maio, and F. Ricci, "Guided wave propagation and scattering for structural health monitoring of stiffened composites," *Composite Struct.*, vol. 184, pp. 568–580, Jan. 2018.

[22] R. Mijarez and P. Gaydecki, "Automatic guided wave PPM communication system for potential SHM of flooding members in sub-sea oilrigs," *Smart Mater. Struct.*, vol. 22, no. 5, May 2013, Art. no. 055031.

[23] M. Mitra and S. Gopalakrishnan, "Guided wave based structural health monitoring: A review," *Smart Mater. Struct.*, vol. 25, no. 5, May 2016, Art. no. 053001.

[24] J. Moll, L. De Marchi, and A. Marzani, "Transducer-to-transducer communication in guided wave based structural health monitoring," in *Proc. 19th World Conf. Non-Destructive Testing*, Munich, Germany, 2016, pp. 1–8.

[25] J. Moll, M. Mälzer, N. Testoni, L. De Marchi, and A. Marzani, "Experimental analysis of digital data communication in intelligent structures using Lamb waves," in *Proc. Struct. Health Monitor.*, Sep. 2017, pp. 1654–1661.

[26] J. Moll, L. De Marchi, C. Kexel, and A. Marzani, "High resolution defect imaging in guided waves inspections by dispersion compensation and nonlinear data fusion," *Acta Acustica United Acustica*, vol. 103, no. 6, pp. 941–949, Nov. 2017.

[27] J. Moll, C. Kexel, and M. Mäzler, "Complex intelligent structures with data communication capabilities," in *Proc. 9th Eur. Workshop Structural Health Monitor.*, Manchester, U.K., 2018, pp. 1–7.

[28] J. Moll, C. Kexel, H. Milanchian, M. B. Bhavsar, and J. H. Barker, "Ultrasound bone fracture sensing and data communication: Experimental results in a pig limb sample," *Ultrasound Med. Biol.*, vol. 45, no. 2, pp. 605–611, Feb. 2019.

[29] I. Mueller, J. Moll, K. Tschoke, J. Prager, C. Kexel, L. Schubert, Y. Lugovtsova, M. Bach, and T. Vogt, "SHM using guided waves-recent activities and advances in germany," in *Proc. Struct. Health Monitor.*, Nov. 2019, pp. 1–4.

[30] K. Neuschwander, J. Moll, V. Memmolo, M. Schmidt, and M. Bücker, "Simultaneous load and structural monitoring of a carbon fiber rudder stock: Experimental results from a quasi-static tensile test," *J. Intell. Mater. Syst. Struct.*, vol. 30, no. 2, pp. 272–282, Jan. 2019.

[31] J. Saniie, B. Wang, and X. Huang, "Information transmission through solids using ultrasound invited paper," in *Proc. IEEE Int. Ultrason. Symp. (IUS)*, Oct. 2018, pp. 1–10.

[32] N. Testoni, L. De Marchi, and A. Marzani, "Detection and characterization of delaminations in composite plates via air-coupled probes and warped-domain filtering," *Compos. Struct.*, vol. 153, pp. 773–781, Oct. 2016.

[33] N. Testoni, L. D. Marchi, and A. Marzani, "A stamp size, 40ma, 5 grams sensor node for impact detection and location," in *Proc. Eur. Workshop SHM*, 2016, pp. 1–8.

[34] G. Trane, R. Mijarez, R. Guevara, and A. Baltazar, "Guided wave sensor for simple digital communication through an oil industry multi-wire cable," *Insight - Non-Destructive Test. Condition Monitor.*, vol. 60, no. 4, pp. 206–211, Apr. 2018.

[35] G. Trane, R. Mijarez, R. Guevara, and D. Pascacio, "PPM-based system for guided waves communication through corrosion resistant multi-wire cables," *Phys. Procedia*, vol. 70, pp. 672–675, 2015.

[36] O. Zienkiewicz, R. Taylor, and J. Zhu, *Finite Element Method: Its Basis Fundamentals*. Amsterdam, The Netherlands: Elsevier, 2013.

[37] Y. Wang, G. Wang, D. Wu, Y. Wang, B. Miao, H. Sun, and X. Qing, "An improved matching pursuit-based temperature and load compensation method for ultrasonic guided wave signals," *IEEE Access*, vol. 8, pp. 67530–67541, 2020.

CHRISTIAN KEXEL received the M.Sc. degree from Goethe University Frankfurt, Germany, where he is currently pursuing the Ph.D. degree in physics. His research interests include signal processing of ultrasonic guided waves.

NICOLA TESTONI received the M.Sc. degree in microelectronics and the Ph.D. degree in information technology from Bologna University in 2004 and 2008, respectively. He is currently an Adjunct Professor with the Department of Electrical, Electronic, and Information Engineering "Guglielmo Marconi," Bologna University. His research interests include guided waves, analog circuit design, non-linear signal processing, wavelet theory and applications, neural signal denoising, and event sorting.
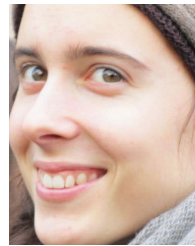
FEDERICA ZONZINI (Student Member, IEEE) received the B.S. and M.S. degrees in electronics engineering from the University of Bologna, Italy, in 2016 and 2018, respectively. She is currently pursuing the Ph.D. degree in engineering and information technology for structural and environmental monitoring and risk management with the University of Bologna. Her main research interests include advanced signal processing techniques for structural health monitoring application, encompassing spectral analysis, graph signal processing, data-fusion, compressive sensing, and damage assessment.

JOCHEN MOLL received the Dipl.-Ing. and Ph.D. degrees in mechanical engineering from the University of Siegen, Germany, in 2007 and 2011, respectively. He is currently a Postdoctoral Research Assistant with Goethe University Frankfurt, Germany. His research interests include non-destructive testing, structural health monitoring, and signal processing techniques. His research profile is located in http://www.jochenmoll.de.

LUCA DE MARCHI (Member, IEEE) is currently an Associate Professor in electronics with the Department of Electrical, Electronic, and Information Engineering, University of Bologna, Italy. He has authored or coauthored more than 140 articles in international journals or in proceedings of international conferences. He holds two patents. His current research interests are in multiresolution and adaptive signal processing, with a particular emphasis on structural health monitoring applications.

• • •